Journal Pre-proof

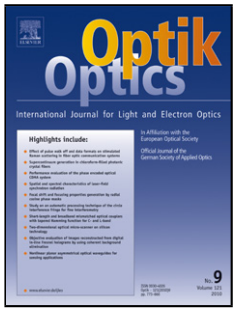

Simulation, statistical modeling, and optimization of CO_2 laser cutting process of polycarbonate sheets

Mahmoud Moradi, Mojtaba Karami Moghadam, Mahmoud Shamsborhan, Zeinab Malekshahi Beiranvand, Alireza Rasouli, Mahdi Vahdati, Arash Bakhtiari, Mahdi Bodaghi

PII: S0030-4026(20)30768-3

DOI: https://doi.org/10.1016/j.ijleo.2020.164932

Reference: IJLEO 164932

To appear in: *Optik*

Received Date: 6 March 2020

Revised Date: 9 May 2020

Accepted Date: 10 May 2020

Please cite this article as: { doi: https://doi.org/

Simulation, Statistical Modeling, and Optimization of CO_2 Laser Cutting Process of Polycarbonate Sheets

Mahmoud Moradi [1, 2, *], Mojtaba Karami Moghadam [1, 2], Mahmoud Shamsborhan [3, 4], Zeinab Malekshahi Beiranvand [5], Alireza Rasouli [1, 2], Mahdi Vahdati [6], Arash Bakhtiari [1, 2], and Mahdi Bodaghi [7, *]

[1] Department of Mechanical Engineering, Faculty of Engineering, Malayer University, Malayer, Iran
[2] Laser Materials Processing Research Centre, Malayer University, Malayer, Iran
[3] Department of Engineering, Mahabad Branch, Islamic Azad University, Mahabad, Iran
[4] Department of Mechanical Engineering, University of Zakho, Kurdistan Region, Iraq
[5] Department of Materials science and Engineering, Tarbiat Modares University, Tehran, Iran
[6] Faculty of Mechanical and Mechatronics Engineering, Shahrood University of Technology, Shahrood, Iran
[7] Department of Engineering, School of Science and Technology, Nottingham Trent University, Nottingham, United Kingdom

*Corresponding authors: mahdi.bodaghi@ntu.ac.uk (M. B.); moradi@malayeru.ac.ir (M. M.)

Highlights:

- Simulation of CO_2 laser cutting of polycarbonate injected sheets by the DOE approach
- Developing governing equations on thermal fields and boundary conditions
- Modeling of the heat source by selecting of an appropriate Gaussian distribution
- Laser power, focal plane position and cutting speed considered for the DOE analysis
- Optimizing the laser cutting simulation process

Abstract

Laser cutting well-known as a manufacturing process is a rapid, repeatable, and reliable method that is frequently used for cutting various materials such as thermoplastics. Due to their physical and chemical properties such as fatigue resistance, high toughness, and re-melting properties, thermoplastics such as polycarbonate are widely used in automotive parts, electronics, etc. In this study, a numerical simulation of the laser cutting process by a finite element method is developed. The sample simulated in this research is a 3.2 *mm* thick Polycarbonate sheet that is subjected to the laser cutting process by a low power continuous CO_2 laser. The effects of the laser cutting process parameters such as laser power, cutting speed, and laser focal plane position on the top and bottom kerf width, top heat-affected zone, the ratio of upper kerf width to lower kerf width and taper kerf are investigated by statistical techniques of variance analysis. Choosing an appropriate Gaussian distribution is studied as

well. The results show that the laser scanning speed has a significant effect on the top kerf width. By choosing a cutting speed of 20 *mm/s* and a focal length of -3, the taper kerf is minimized. By increasing the laser cutting speed from 4 to 20 *mm/s* and decreasing the laser power from 50 to 20 Watts, the heat-affected zone decreases. The developed analysis can predict the depth of kerf in a continuous mode for different values of laser power, speed, and laser focal plane.

Keywords: polycarbonate; laser cutting; optimization; finite element method; statistical modeling; experimental validation

Introduction

Laser cutting is a two-dimensional machining process that involves the removal of materials by high-intensity beam focusing on the workpiece. The laser beam melts or evaporates the workpiece in the thickness or depth direction of materials and creates a kerf wall. Then the molten material is blown away using an assistant gas. In the laser machining, unlike traditional methods, material-removing is almost conducted without applying any force. This feature makes the laser machining suitable for delicate and brittle parts on which too much force should not be applied. Ultra-thin kerf width, which saves a significant amount of materials, is another feature of the laser cutting. In the laser machining, the final surface quality can be achieved in one step, and no further finishing operations are needed to smooth and clean the surface. Minor noise pollution, shallow heat-affected zone, very high cutting speed, and ease of automation are the other features of the laser cutting. Lasers are capable of cutting a wide range of brittle or ductile, conductive or nonconductive, hard or soft materials. Table 1 compares the laser cutting process with the other cutting processes from different aspects.

Table 1- Comparison of different cutting process types

Quality	Laser	Wire cut EDM	Ultrasonic	Abrasive fluid jet	Plasma
Speed	✓	☒	☒	☒	✓
Kerf quality	✓	✓	✓	✓	☒
Kerf width	✓	✓		✓	☒
Wear of tool	✓	☒	☒	✓	✓
Metal and non-metal	✓	☒	✓	✓	☒
Heat-affected zone	✓	✓	✓	✓	☒

Polycarbonate (PC) is a transparent polymeric material from the thermoplastic group that is usually made in the form of plates with a flat or dentine surface. This material has excellent optical properties and high impact resistance [2]. The impact resistance of the polycarbonate sheet is 250 times higher than a glass with the same thickness. Various sheets of polycarbonate show scratch resistant like glass, under very tough test conditions. Among the advantages of polycarbonate coating in comparison with glass are its lower cost and lighter weight. Furthermore, its high resistance in contrast to plastic has led to its increasing demand in the industry. Chemical resistance to many organic acids and mineral oils, excellent flexibility, and low thermal conductivity (suitable thermal insulation) have led to the increasing expansion of polycarbonate. Polycarbonate is highly resistant to Ultraviolet (UV) rays due to its anti-UV coating. Its color also does not change in the sun's radiation, consequently retains its transparency for a long time. These properties have led to the use of polycarbonate in the automotive, health, and medical, electrical, and computer industries. So far, various studies have been done on the laser cutting process. These studies involve experimental activities on metallic and non-metallic materials [3, 4, 5, 6, 7]. In many of these studies, process modeling has been done using statistical methods and neural networks. Due to the problems and costs of experiments, in many other studies, the process modeling has been done by numerical and analytical techniques.

By studying previous studies, a set of parameters and quantities evaluated in different studies are shown in Figure 1. Then, the latest research on laser cutting of polymer materials is described.

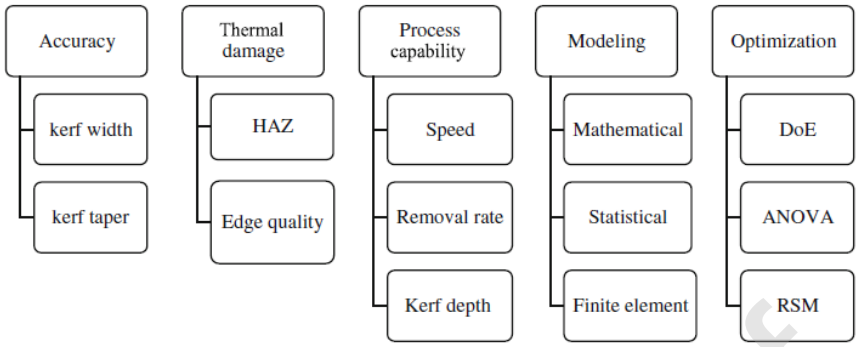

Figure 1 – Aspects and quantities investigated in the previous studies on the laser cutting process [8].

In 2019, Aref Varsey et al. [9] studied the taper kerf resulting from laser cutting on Polymethyl methacrylate (PMMA), using statistical methods. In this study, the effect of laser power parameters, the scanning speed, and the number of sweep steps was investigated using analysis of variance. Experimental studies using statistical methods on the cutting processes were carried out by Haddadi et al. [10]. Chen et al. [11] used an experimental design technique (Taguchi method) to enhance the surface quality of microchannels obtained by laser cutting on PMMA materials. In this study, power parameters, the scanning speed, and the time of process were optimized to achieve less roughness. They were able to make an average roughness of 110 nm. Saleh Jassim et al. [12] conducted studies on the cutting and drilling of the high-density polyethylene pipes by CO_2 laser. In this research, the effect of injected gas during the process, laser power, and the thickness of the workpiece on the kerf width and heat-affected zone were evaluated. Gruska et al. [13] investigated the effect of laser power and laser speed on the surface quality of polycarbonate gears by the Taguchi method. Hoffey et al. [8] summarized the results of research on laser cutting on fiber-reinforced polymer composites. The results show that most studies are focused on the heat-affected zone, width, and depth of kerf. This study demonstrated that short pulses, high speed, low laser intensity, and high pressure of injected gas should be used to achieve the most moderate heat-affected zone. In 2018, Aref Varsi et al. [14] designed algorithms to predict the number of laser scanning steps in laser cutting on PMMA materials to achieve a specific kerf depth. There was a good agreement between the result of the algorithms and the experimental results.

In the engineering fields, different methods are used for tackling problems with high accuracy, and one of the most practical approaches for engineers is finite element method (FEM). It is employed in different areas such as heat transfer, fluid flow, structural analysis, electromagnetic potential, and mass transport. There is a large number of experimental studies on laser cutting, but analytical studies on the nature of this process and its parameters are very limited. Recently, the use of the finite element method for simulating laser cutting

has been expanded. In many studies in this field, the temperature distribution resulting from the laser beam on the surface of the workpiece (metal and non-metal) has been analyzed [15-19]. In some studies, the kerf depth, taper kerf, and surface quality of kerf have been investigated, too [20-23]. In 2019, Benton et al. [24] evaluated the effect of laser micromachining parameters and thermal properties of the workpiece on the kerf depth resulting from this process, for the fabrication of microchannels on polymeric PMMA materials by finite element methods (COMSOL software package). In 2019, Jiang Nam Li et al. [25] used a numerical solution method (COMSOL software package) to determine the effect of the laser speed and laser power on the laser cutting process of PMMA materials. In this modeling, the Arbitrary-Eulerian-Lagrangian method technique was used. Moradi and Golchin [26] chose a suitable Gaussian distribution for modeling in the laser drilling simulation. New combined techniques with Laser machining have been developed in recent years to reduce the thermal damage and prevent the formation of the resolidified layer. The laser micromachining method on the ice layer is one of the new techniques. In 2019, Macklow developed a thermal model to examine this technique more accurately [27]. Also, in 2019, Choi et al. [28] presented a three-dimensional thermo-elastic model to understand the method proposed to solve the problem of laser cutting of brittle materials. One of the gaps in previous studies that have been examined in the present study is choosing a suitable Gaussian distribution to simulate laser cutting. Furthermore, numerous brilliant studies were conducted by FEMs in many fields [29-34]. Reviewing previous numerical studies shows that statistical methods have not been used in these studies to investigate the effect of parameters and extract the regression model. Table 2 illutreates some studies on cutting processes investigated by various methods.

In the present study, the effects of process parameters including cutting speed, laser power, focal length on the kerf width, the top and the bottom kerf width, taper kerf, and heat-affected zone are investigated by analysis of variance. The optimal condition for each output is also determined. Due to the polycarbonate properties, the laser cutting process results in color opacity (yellowness of plane) as well as burnt edges. Appropriate choosing of laser cutting process parameters increases the kerf quality as well as eliminating burnt edges in this process. The widespread use of polycarbonate in the industry highlights the importance of this study.

Table 2- Different cutting processes applied in various studies

Authors	Materials	Method	Goal(s)	Year	Ref.
Varsi et al.	Polymethyl methacrylate	Statistical methods	Parameters optimization	2019	9
Haddadi et al.	Polystyrene	Response surface method	Improving the Laser cutting condition	2019	10
Chen et al.	Polymethyl methacrylate	Orthogonal experimental method	Laser cutting optimization	2017	11
Saleh Jassim et al.	Poly ethylene	Experimental Study	Thermal conductivity and polymer absorption of the (CO2) laser	2019	12
Sihn et al.	Polymer Matrix composites	Finite Element Method	Model for Temperature Evolution	2019	15
Yilbas et al.	Inconel 803 Alloy	Finite Element Method	Analysis of Thermal Stress Field	2019	17
Amara et al.	Stainless steel	Volume-of-fluid method	Simulation of the workpiece kerf formation with CO2 laser	2016	18
Ayed et al.	Ti6Al4V titanium alloy	Finite Element Method	Controlling the reduction of the cutting force	2014	20
Meško et al.	Low alloy steel	Finite Element Method	Simulation of laser cutting process	2018	21
Kheloufi et al.	Mild steel	Volume of fluid method	Simulation of Transient 3D Temperature in Laser Cutting	2015	22
Li et al.	Polymethyl methacrylate	Arbitrary Lagrangian Eulerian method	Effects of laser machining parameters	2019	25
Choi et al.	silicon wafer	Finite Element Method	The mechanism of crack propagation	2019	28
Li et al.	Carbon fiber reinforced plastic	Finite Element Method	Defect characteristics and strain distribution following fiber laser cutting	2020	35
Kaselouris et al.	AISI H-13 Steel	Finite Element Method	Simulation of laser cutting process	2020	36

2- Finite element simulation

Due to many parameters affecting the laser cutting process, changes in material properties during machining resulting from thermal variations, and other complexities in the process, achieving accurate estimation of the amount of material removal is relatively complex and challenging and analytical methods can only be done with a lot of simplifying assumptions. Therefore, a finite element simulation of the laser cutting process can be considered as an appropriate method to predict the thermomechanical behavior of this process.
The aim of thermal modeling is the calculation of thermal distribution in the kerf of the sample. Therefore, all the thermal effects of the workpiece, the laser, and gas jet are involved in the results. Also, the thermal parameters of the workpiece material are determinant in the thermal field results. To create an accurate thermal model for the laser cutting process, the following considerations are necessary:

- Heat transfer from the surface of the melt pool and the workpiece to the surrounding environment is carried out by two mechanisms of convection and radiation.
- Large thermal gradients occur in the melt pool.
- Thermal and mechanical properties of steel, including heat conductivity, specific heat, density, Young's modulus, yield stress, and plastic strain, have been used as a function of temperature.
- To consider the effect of heat loss resulting from gas jet, the convection coefficient of 1000 W/m^2k is applied for kerf zone.
- Specific latent heat is considered as an incremental amount of specific heat in the phase change region.
- The laser beam is modeled as a heat source with Gaussian-distributed heat flux.

2-1- Governing equations on thermal fields and boundary conditions

The basic equation of thermal conduction denotes the thermal distribution in the workpiece based on the law of energy conservation, the capacity of the workpiece to store this energy, and the heat transfer rate across the boundaries according to the Fourier law. The three-dimensional heat transfer in the Cartesian coordinates is expressed as equation 1 [37-38]:

$$\frac{\partial}{\partial x}\left(k_x(T)\frac{\partial T}{\partial X}\right)+\frac{\partial}{\partial y}\left(k_y(T)\frac{\partial T}{\partial y}\right)+\frac{\partial}{\partial z}\left(k_z(T)\frac{\partial T}{\partial z}\right)=\rho(T)C(T)\frac{\partial T}{\partial t} \quad (1)$$

where $k_x(T)$, $k_y(T)$ and $k_z(T)$ represent non-isotropic thermal conductivity coeficients, $\rho(T)$ is heat-dependent density, $C(T)$ is heat-dependent heat capacity, and t is time. For an isotropic material, the thermal conductivity is equal, along with all three coordinate directions. Equation 1 is rewritten in a matrix form as equation 2:

$$\rho C\frac{\partial T}{\partial x}=\{L\}^T([D]\{L\}T) \quad (2)$$

As stated in the assumptions, heat transfer at the surface of the workpiece is considered as thermal convection and radiation. By solving the equations governing the transient heat transfer in the workpiece, with determined boundary conditions and certain initial conditions, the temperature field in the model is obtained. In the laser cutting, because of the transient process and mass removal phenomena, as well as having a wide temperature range coupled with the phase changes and the dependence of material properties on temperature, these equations take on a very complicated nonlinear form that solving them through mathematical relationships is not easy. Thus, for modeling of the laser cutting, a finite element method will be developed.

2-2- Simulation method

First, the thermal model is presented to calculate the heat-affected zone. Then the measurement of the top and bottom kerf of the workpiece resulting from laser radiation, will be described. After applying heat flux to the surface of the workpiece, elements whose temperature is higher than the melting temperature of the material are removed from the workpiece surface.

To simulate this process, the element birth and dead technique is used. That means elements whose temperatures are higher than the melting temperature, are death. Figure 2 shows the three-dimensional cross-section of the geometrical model with dimensions of 80*175*3.2 *mm*. It is obvious that the side of the workpiece, which is influenced via laser treatment, has a fine mesh. Due to the high-temperature gradients near the kerf zone, the number of elements in this region is higher than the number of elements in the farther points from the kerf zone. Connecting the fine elements to the large elements is done through pyramid-shaped intermediate elements.

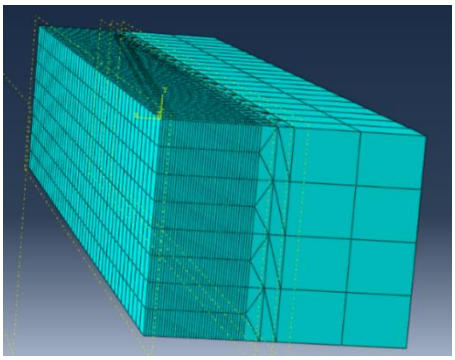

Figure 2- A view of mesh detail of the model geometry

The material used in this study is a colorless U1100 granola polycarbonate sheet with temperature-dependent thermal properties. Therefore, in the simulation of heat transfer processes, it is necessary to apply these properties as a function of temperature. The temperature-dependent thermal properties of polycarbonate are presented in Table 3.

Table 3- Physical and thermal properties of polycarbonate U1100 at different temperatures [7].

Temperature (°C)	Density (g/cm3)	Specific heat (j/g.k)	Coefficient of thermal conductivity (w/m.k)
25	1.193	1.32	0.199
43	1.191	1.33	0.203
69	1.188	1.35	0.206
93	1.185	1.37	0.211
118	1.181	1.39	0.215
142	1.170	1.47	0.212
167	1.512	1.49	0.211
192	1.138	1.50	0.213
221	1.111	1.53	0.222
246	1.097	1.53	0.226
271	1.070	1.550	0.232
298	1.057	1.557	0.237

2-2-1- modeling of the heat source (selecting of an appropriate Gaussian distribution)

In the laser cutting simulation, the Gaussian distribution is often used as an optimal distribution for modeling the laser heat flux. The Gaussian distribution has a unique geometric shape, but the Gaussian distribution presented for simulating laser cutting may be different in some parameters. In this study, three different Gaussian distributions are used for simulation and their results are compared with experimental results [2].

To obtain the appropriate Gaussian distribution, three cases of experimental results are considered as a baseline, and three different Fortran codes are written for the three different Gaussian distributions. Simulations are then performed under conditions of these experiments for each of the Gaussian distributions. Due to the difference between the results of the first Gaussian distribution and the experimental results, the suitability of the Gaussian Distribution No. 1 is confirmed. Since the ABAQUS software is not capable of moving the heat source onto the model as well as the heat flux distribution in the Gaussian form, an ABAQUS Dflux subroutine in the Fortran programming language is developed in this study. Applying Gaussian heat flux results in equation 3 and 4 as:

$$Q = \frac{2P}{\pi r_0^2 H} e^{1-(r/r_0)^2}\left(1-\frac{y}{H}\right) \quad (3)$$

$$r(x,z,t) = \sqrt{(z - vt - z_{in})^2 + x^2} \quad (4)$$

where p is the absorbed laser energy, r_0 is the radius of the laser beam, r is the radial distance from the laser beam axis, H is the thickness of the workpiece, and y is the current coordinate in-depth direction. The radial distance from the laser beam axis is calculated from equation 4, where v is the laser velocity, z_{in} is the initial coordinate of the laser in cutting direction, x and y are the current coordinates at any time, during the laser movement [39]. Figure 3 also shows an overview of the Gaussian distribution used in this study. The peak of Gaussian distribution has a significant effect on the laser cutting process because it has a high temperature in this area. By this property, the workpiece is cut very smoothly.

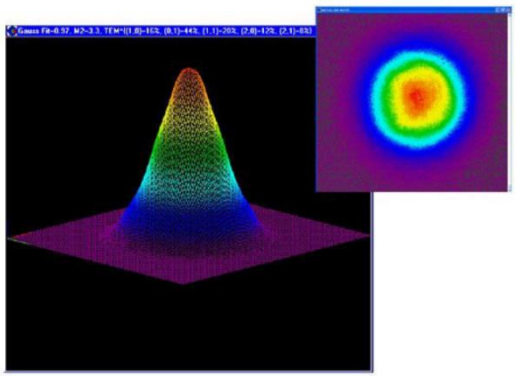

Figure 3- Gaussian distribution of the laser beam

The simulated laser radiation has a maximum power of 50 Watts and a wavelength of 1064 µm. In the thermal model, DCC3D8 elements are used. This element, is a rectangular cubic 8-noded element with a linear connection whose only degree of freedom is temperature, and it can be used in both stable and transient thermal analyses. Due to the symmetry of the model along the kerf line, the heat transfer is also symmetrical to this line, and there are no boundary conditions for it. In other words, it is considered isolated. For other outer boundaries of the sheet, convection and radiation boundary conditions are used. The radiation coefficient and the convection coefficient are considered equal to 0.6 and 30 W/mK, respectively. For the floor of the workpiece that is attached to the ground, the convection coefficient is 100 W/mK. The ambient temperature is also considered to be 25 $^{\circ}$C. Element birth and death technique is used to simulate the material removal during the cutting process. This technique is based on deactivating elements of the melt pool during cutting. Thus, by starting machining and applying the heat flux, the elements whose temperature exceeds the melting temperature of the material are deactivated, and do not participate in the calculation. Top kerf width, bottom kerf width, alpha angle, and heat-affected zone are investigated as simulation outputs. How to measure the above parameters is shown in Figure 4. According to Figure 4, the alpha angle, which is shown as α in this figure, is calculated from equation 5 defined as [2]:

$$\alpha = tan^{-1}\left(\frac{\text{Bottom kerf} - \text{Top kerf}}{2 \times thickness}\right) \quad (5)$$

In this equation, Bottom kerf and Top kerf are changeable. Figure 5a shows an overview of the bottom of the model after the thermal simulation. The heat-affected zone of the workpiece is calculated from the thermal analysis. Based on Figure 5a and thermal analysis, laser heat is more effective on top of the workpiece, and this phenomenon happens because of the shape of Gaussian distribution. As mentioned before, the mesh size in this zone is very smaller than the far part of laser treatment, and it helps to increase the accuracy of the calculation in this area. Figure 5b also illustrates an overview of the model after the death of the elements where the top and the bottom kerf width are calculated from this analysis.

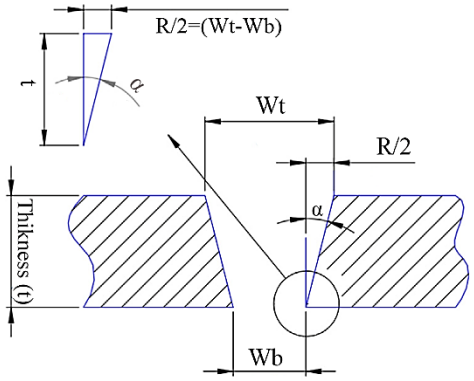

Figure 4- Schematic of the geometrical profile in the cross-section of kerf [2].

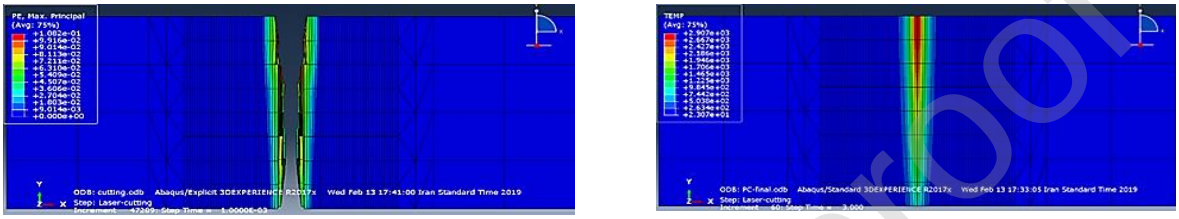

(b) (a)

Figure 5- a) The view of the bottom of the model after thermal simulation, b) the view of the bottom of the model after the death of the elements.

A comparison of the experimental results [2] with three different Gaussian distributions is presented in Table 4. Due to error values obtained from comparing calculations with experimental results for all three Gaussian distributions, the Gaussian Distribution No. 1 is used to perform other simulations.

Table 4- A comparison between experimental results and different Gaussian distributions in the simulation

No.	Cutting speed mm/s	Laser Power W	FPP mm	Top Kerf (experimental)	Bottom kerf (experimental)	Gaussian distribution #1		Gaussian distribution #2		Gaussian distribution #3	
						Top kerf Error %	Bottom kerf Error %	Top kerf Error %	Bottom kerf Error %	Top kerf Error %	Bottom kerf Error %
1	6	35	-3	265	163	13	8	22	19	19	19
2	10	30	-3	312	163	12	11	25	21	18	17
3	10	20	0	306	287	10	7	27	24	16	15

2-3- Validation of the model

After selecting the appropriate Gaussian distribution and creating the model to simulate the laser cutting process of polycarbonate, the model is validated using experimental results reported in Ref. [39]. A comparison between simulation and experimental results is presented in Table 5.

Table 5- The comparison between simulation and experimental results

No.	Inputs			Top kerf			Bottom kerf		
	Power (P)	Speed (mm/s)	FPP (mm)	Experimental (µm)	Simulation (µm)	Percent error (%)	Experimental (µm)	Simulation (µm)	Percent error (%)
1	35	6	0	612.25	600	2	428.57	375	12.49
2	35	6	-1	518.37	600	-15.7	363.26	300	17.4
3	35	6	-2	424.49	375	11.65	306.12	300	1.9
4	35	6	-3	265.31	225	15.19	163.26	150	8.12
5	35	6	-4	285.71	300	-5	204.08	225	-10.25

2-4- Design of simulation experiments

After validating the model and proving its performance in predicting the laser cutting process, 15 simulations were done based on the response surface methodology (RSM). In these 15 simulations, three parameters, including the laser power, laser focal plane position, and laser cutting speed, are considered as inputs data. The reason for selecting these three inputs is that in experimental conditions, the laser source is capable of changing these three parameters. Also, top kerf width, bottom kerf width, alpha angle, and heat-affected zone are selected as output parameters. Table 6 shows the variation ranges of input parameters. Also, the matrix layout of the experiments, along with the values of the output results, is presented in Table 7. The star sign in Table 7 indicates that the cutting process is not performed under the relevant conditions. The position of the focal length is demonstrated in Figure 6. Focal plane position (FPP) was on the top of the workpiece where it was set as zero position. Also, the bottom and top of FPP were considered negative and positive, respectively.

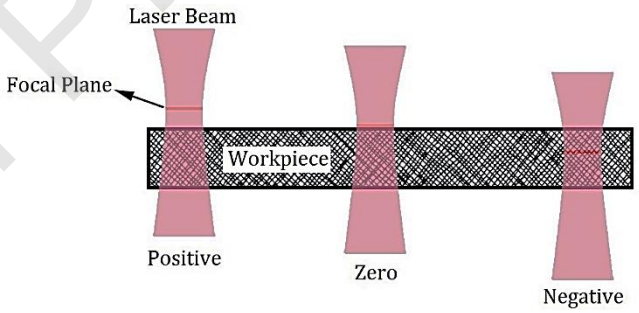

Figure 6- Diagram of the laser focal position.

Table 6- The variations range of input parameters in the designed experiments

Parameters	Sign	Unit	-2	-1	0	1	2
Speed	S	[mm/s]	4	8	12	16	20
Power	P	[w]	30	35	40	45	50
Focal plane position	FPP	[mm]	-3	-2	-1	0	1

Table 7- Matrix layout of experiments

No.	Inputs			Outputs			
	Speed (mm/s)	Power (W)	FPP (mm)	Top Kerf (µm)	Bottom kerf (µm)	HAZ (µm)	Alpha Angle (°)
1	8	45	0	375	262.5	1.428571	2.013475
2	20	40	-1	300	225	1.333333	1.342624
3	12	40	-1	225	150	1.5	1.342624
4	12	40	1	*	*	*	*
5	12	40	-3	187.5	187.5	1	0
6	16	35	-2	337.5	300	1.125	0.671404
7	16	35	0	300	150	2	2.683775
8	8	35	-2	525	375	1.4	2.683775
9	8	35	0	412.5	300	1.375	2.013475
10	16	45	0	337.5	225	1.5	2.013475
11	12	50	-1	262.5	150	1.75	2.013475
12	16	45	-2	300	375	0.8	-1.34262
13	4	40	-1	750	450	1.666667	5.355825
14	12	30	-1	150	150	1	0
15	8	45	-2	600	375	1.6	4.02199

3- Results and discussion

In this section, statistical analysis and analysis of three inputs parameters including laser power, laser focal plane position, and laser cutting speed on output parameters (top kerf width, bottom kerf width, the ratio of top kerf width to bottom kerf width, and heat-affected zone) are presented. Each section also provides tables for the analysis of variance, regression equation, RSM graphs, and standard curves for each output.

3-1- Top kerf width

Table 8 shows a modified variance analysis of the model for top kerf width. This table is obtained after removing ineffective parameters. P-value indicates the effect of each parameter on the top kerf width. The calculation of the probability value is based on the assumption of zero. For each parameter, if the P-value is less than 0.05, it means that the parameter is effective on the top kerf width. It also indicates the significance of the model. Equation 6 is the regression equation for the top kerf width. In this equation, and also the following equation, some parameters are shown by their abbreviations such as speed (S), focal plane position (FPP), and power (P). The values of R-sq and R-sq (adj) are the amount of data coverage by the regression equation. Figure 7 illustrates the curve of residuals distribution for the top kerf width. It can be seen that the residual is scattered around the oblique line, and shows a normal distribution; therefore, the final extracted regression model is also found a suitable model for predicting and investigating the effects of the parameter.

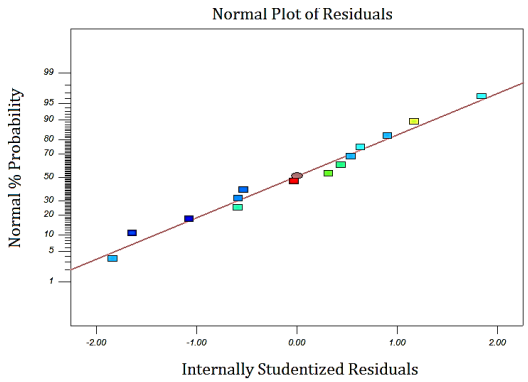

Figure 7- Residuals curve for the response of the top kerf width

Table 8- The modified variance analysis for the top kerf width

Source	Sum of Squares	Df	Mean Square	F Value	P value
Model	38045848	5	7609170	8.8446	0.0041
A-Speed	20073231	1	20073231	23.33234	0.0013
B-Power	381489.2	1	381489.2	0.443428	0.5242
C-FPP	451547.9	1	451547.9	0.524862	0.4894
AC	1957151	1	1957151	2.274916	0.1699
A^2	15622610	1	15622610	18.15911	0.0028
Residual	6882545	8	860318.1		
Total	44928392	13			
R-sq: 84.6811% R-sq(adj): 75.1068%					

$$(\text{Top kerf})^{1.35} = 10111.18637 - 1441.953815\,S + 30.88240787\,P - 1682.225816\,FPP + 123.653719\,S\times FPP + 53.56615792\,S^2 \quad (6)$$

The cutting speed and squared laser power have the highest effect on top kerf width, respectively, and the focal length and laser power do not have much effect. Figure 8, illustrates the effect of different parameters on the top kerf width. In this curve, the high slope (positive or negative) indicates that the above parameter has a significant effect on the main parameter (here, the top kerf width). Obviously, by increasing the laser power, the top kerf increases, and FPP has an inverse effect. By increasing FPP, the top kerf reduces because the area influenced via laser beam is further away than the close distance of FPP and workpiece position.

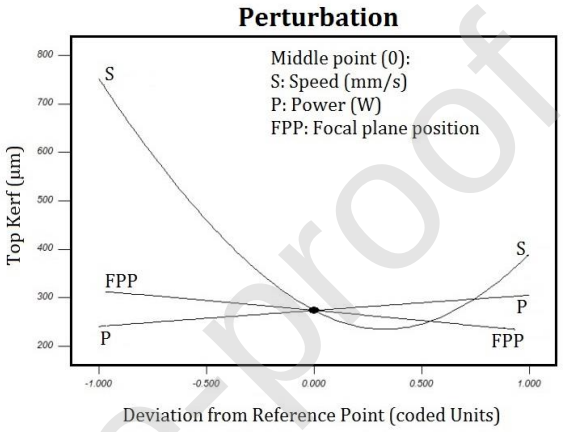

Figure 8- The effect of different parameters on the top kerf width

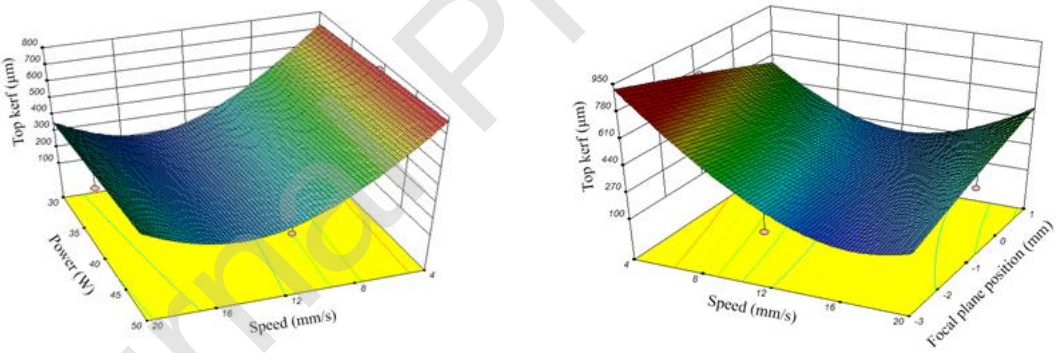

(a) (b)

Figure 9- Top kerf RSM curve a) for cutting speed and laser focal plane position, b) for laser power and laser speed

As shown in Figure 9a, the highest top kerf width occurs at a speed of 4 mm/s, and a focal plane distance of -3 from the workpiece surface. In Figure 9a, the laser power is the average range of 40 W. As the laser cutting speed increases from 14 mm/s, the top kerf width decreases due to the interaction between the effects of cutting speed and laser power. It is also found from Figure 9b that due to the interaction between the effect of cutting speed and laser power, the highest top kerf width occurs at a speed of 4 mm/s and power of 50 W. This phenomenon can be justified by the amount of the heat input. Equation 7 represents the amount of heat input based on the laser power and speed [40].

$$\text{Heat input} = \frac{\text{Power}}{\text{Speed}} \quad (7)$$

As the laser power increases, and the cutting speed decreases, the heat input increases, and more of the workpiece melt, resulting in a higher top kerf width. In Figure 9b, the missing parameter is the focal plane distances with an average range of -1. As the laser cutting speed increases from 14 mm/s, the top kerf width has an increasing inverse trend that is justified by the interaction between the cutting speed effect and the laser FPP effect.

3-2- The bottom kerf width

According to Table 9, the parameters of cutting speed and laser FPP have the greatest effect on the bottom kerf width, respectively. Also, Equation 8 shows the regression relation for the bottom kerf width.

Source	Sum of Squares	Df	Mean Square	F-Value	p-value Prob > F
Model	6.425553	3	2.141851	1.287573	0.0315
A-Speed	4.697476	1	4.697476	2.823885	0.0238
B-Power	0.154891	1	0.154891	0.093113	0.6665
C-FPP	1.573186	1	1.573186	0.94572	0.0437
Residual	16.6348	10	1.66348		
Total	23.06035	13			
R-sq: 73.3426% R-sq(adj): 60.9646%					

Table 9- The modified variance analysis for the bottom kerf width

$$(\text{Bottom kerf})^{0.39} = 9.050238377 - 0.135460379\ S + 0.019678123\ P - 0.366464717\ FPP \quad (8)$$

Figure 10 illustrates the effect of different parameters on the bottom kerf width. The laser FPP, cutting speed, and laser power are linearly correlated with the bottom kerf width, and the maximum value for the bottom kerf width is 350 µm, which occurs at a cutting speed of 4 mm/s and a power of 20 W. According to Figure 10, the laser power has a direct relationship with the bottom kerf width. As the laser power increases, the bottom kerf width increases by 17%. As can be seen from figure 10, the laser cutting speed is an effective parameter for the bottom kerf width. With reducing the laser cutting speed, the bottom kerf width will have an increase due to the increased interaction time of the laser beam with the workpiece. It is observed that by reducing the laser cutting speed from 20 mm/s to 4 mm/s, the bottom kerf width increases around 45%.

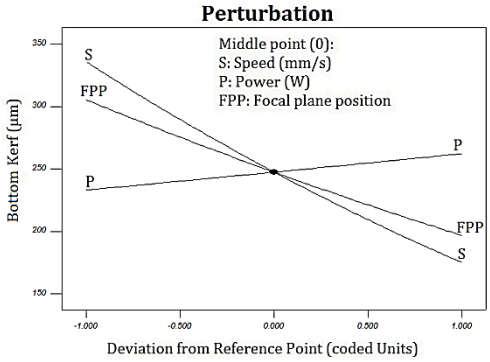

Figure 10- The effect of different parameters on the bottom kerf width

As seen in Figure 10, it can be found that the focal plane position has a prominent influence on the bottom kerf width. The farther the laser FPP from the workpiece surface towards the depth of workpiece, the higher the bottom kerf width becomes. That is because the focus of laser energy is positioned at the laser FPP, and the closer it is to the depth of the workpiece, the bottom kerf width increases. Also, by increasing the laser FPP, the bottom kerf width increases by 30%.

3-3- Heat-affected zone

Table 10 presents the modified variance analysis for the heat-affected zone. Laser cutting speed and laser power have the most effect on the heat-affected zone, and the laser FPP can almost be considered as an effective parameter.

Table 10- The modified variance analysis for heat-affected zone.

Source	Sum of Squares	Df	Mean Square	F Value	P value
Model	0.001917	4	0.000479	4.691289	0.0254
A-Speed	0.000773	1	0.000773	7.569327	0.0224
B-Power	0.000626	1	0.000626	6.124729	0.0353
C-FPP	0.000439	1	0.000439	4.292717	0.0682
AC	7.95E-05	1	7.95E-05	0.778385	0.4006
Residual	0.000919	9	0.000102		
Cor Total	0.002836	13			
R-sq: 67.5853% R-sq(adj): 53.1787%					

Also, the regression equation for the heat-affected zone is given in equation 9:

$$(HAZ)^{-0.22} = 0.29168069 + 0.002526117\ S - 0.001250666\ P - 0.003339668 FPP + 0.00078817\ S \times FPP \quad (9)$$

Figure 11 demonstrates the effect of different input parameters on the heat-affected zone. The results reveal that the cutting laser speed and laser power have a significant effect on the heat-affected zone. By increasing FPP in the laser cutting process, the amount of HAZ area reduces because the laser beam could make a wider zone treatment, and the concentration of the laser beam on a particular zone is decreased.

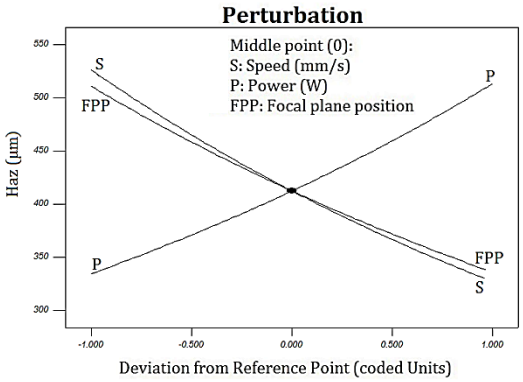

Figure 11- The effect of different parameters on the heat-affected zone

As shown in Figure 11, with increasing the laser power, the area of the heat-affected zone increases by 38%, due to a rise in the energy entering into the surface of the workpiece. According to Figure 11, it is seen that as the cutting speed decreases, the area of the heat-affected zone increases by 40% due to the more absorbed energy by the workpiece at low speeds. Conversely, at high cutting speeds, due to the less energy absorption, the heat-affected zone decreases. Figure 11 displays that as the laser FPP moves deeper into the workpiece, the area of the heat-affected zone increases. By increasing the laser focal plane position, the maximum amount of laser energy is approaching the bottom of the workpiece, creating a more heat-affected zone. Using equation 11, the RSM curves are plotted for the heat-affected zone in Figure 12.

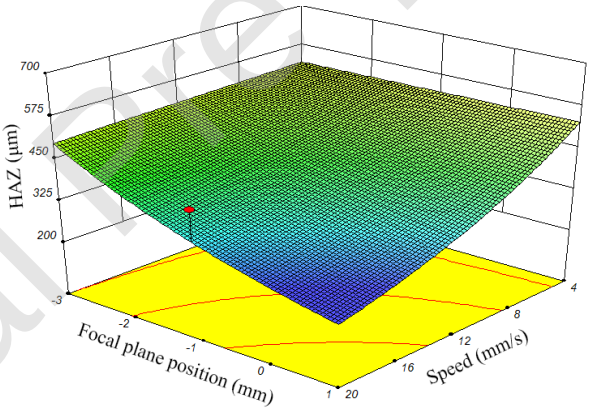

Figure 12- The HAZ response surface diagram of the focal plane position and cutting speed

It can be seen from Figure 12 that both the laser FPP and the cutting speed parameters are effective in the area of heat-affected zone and the lowest heat-affected zone also occurs at the highest FPP (+1) and the maximum laser cutting speed (20 mm/s). As shown, by increasing the cutting speed at the focal plane position of -3, the heat-affected zone does not change significantly, but at the FPP of +1, with increasing cutting speed, the heat-affected zone decreases. That is because at the FPP of -3, all laser energy concentration is within the workpiece, and the cutting speed does not have much effect on the heat-affected zone, in contrast at the focal plane position of +1, the main laser energy concentration is 1 mm above the workpiece surface, and therefore, increasing the laser cutting speed reduces the heat interaction with the surface of the workpiece, and consequently decreases the heat-affected zone.

3-4- **Kerf taper angle**

Table 11 shows the modified variance analysis for the alpha angle. According to P-value, cutting speed is the most effective parameter among the main parameters. And the squared cutting speed (in equation 10) is the single parameter that affects the value of the alpha angle.

Table 11- The modified variance analysis for the alpha angle.

Source	Sum of Squares	Df	Mean Square	F Value	P Value
Model	12.52615	7	1.789451	4.2824	0.0481
A-Speed	4.288691	1	4.288691	10.26342	0.0185
B-Power	1.273761	1	1.273761	3.048283	0.1314
C-FPP	0.560442	1	0.560442	1.341213	0.2908
AB	0.08072	1	0.08072	0.193174	0.6757
AC	1.857274	1	1.857274	4.444711	0.0796
BC	0.454821	1	0.454821	1.088448	0.3370
A^2	3.514305	1	3.514305	8.410212	0.0273
Residual	2.50717	6	0.417862		
Cor Total	15.03332	13			
R-sq: 83.3226% R-sq(adj): 63.8656%					

$$(\text{Alpha angle})^{0.82} = 2.452636097 - 0.417816779\,S + 0.069012384\,P + 0.68302616\,FPP - 0.005022454\,S \times P + 0.120457279\,S \times FPP - 0.047687565\,P \times FPP + 0.025405833\,S^2 \quad (10)$$

Figure 13 illustrates the effect of different input parameters on the alpha angle. As can be seen, the laser cutting speed has a weighty effect on the alpha angle.

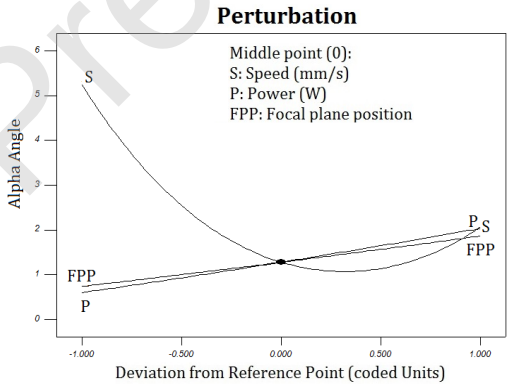

Figure 13- The effect of different parameters on the alpha angle

According to the results presented in Table 11 and Figure 13, the laser power and laser focal plane position have a direct and linear relationship with the alpha angle, and the laser cutting speed has a non-linear relationship with the alpha angle. Also, according to Table 11, the laser power does not affect the alpha angle value. However, according to Figure 13, as the laser power increases, the alpha angle increases too. The reason is that an increase in the laser energy, increases the difference between the top and bottom kerf widths. Figure 13 reveals that the lower laser cutting speed, the more alpha angle increases due to the increase of the laser interaction time with the workpiece. The laser focal plane position does not affect the alpha angle, but Figure 13 shows that as the laser focal length goes to the depth of the workpiece, the alpha angle increases. According to Table 11 and equation 12, which is the regression relation for the alpha angle, the response surface is plotted in Figure 14.

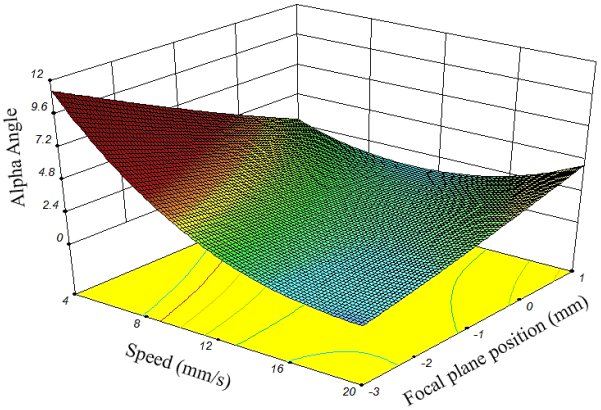

Figure 14- The Taper angle diagram of a response surface for cutting speed and focal plane position

Figure 14 represents that the highest value of the alpha angle occurs at the cutting speed of 4 mm/s, and laser FPP of -3 mm. The lowest amount of the alpha angle occurs at cutting speed of 20 mm/s and laser FPP of 3 mm. At the focal plane position of +1, with increasing the cutting speed up to 14 mm/s, the alpha angle decreases, and at cutting speed of 14 mm/s or higher, the alpha angle increases due to the interaction of the laser effects between the cutting speed and the laser power (average range of 40 W).

4- Optimization

In this study, after the simulations, according to the model given by the design of experiments, the optimization of the process is done by a design expert software, in which the outputs of the simulation process are optimized. The optimization aims are the highest top kerf width, the lowest bottom kerf width, the lowest alpha angle, the kerf ratio of 1, and the lowest heat-affected zone, respectively. In this process, using the optimization results, the simulation of the polycarbonate laser cutting process is repeated. Five optimization criteria are modified by varying the importance of each of the optimal parameters to create a suitable model for simulating the sample, as shown in Table 12. After optimizing the experiments, the simulation results, and the optimization results are compared with the design expert program, and the error percentage for each output response is given in Table 13. According to the obtained results, the error percentage between the simulated samples, and the samples extracted from the software is very low, and this shows the excellent performance of the simulation. Also, Figure 15 shows the over plot, which is the integration of contour plots of each response in the top view of each other. In each part, areas of less importance are shown in gray. The remaining yellow area also represents the final desired region of the input parameters. For example, in Figure 15a, the center of the diagram shows proper output parameters influenced by speed and FPP. As mentioned in the previous sections, the interaction of parameters is an important part of this research, and by these figures, the concept of optimized parameters is shown better.

Table 12- Constraints and criteria of input parameters and responses

Parameter/Response			Goal	Lower	Upper	Importance
Parameters		Scanning speed	in range	4	20	---
		Laser power	in range	30	50	---
		Focal plane position	in range	-3	1	---
[illegible]	Criteria 1	Top Kerf	Maximize	150	750	1

	Bottom kerf	Minimize	150	450	1
	Ratio	1	0.8	2	4
	HAZ	Minimize	262.5	712.5	5
	Alpha Angle	Minimize	0	5.35	1
Criteria 2	Top Kerf	Maximize	150	750	1
	Bottom kerf	Minimize	150	450	3
	Ratio	1	0.8	2	5
	HAZ	Minimize	262.5	712.5	3
	Alpha Angle	Minimize	0	5.35	3
Criteria 3	Top Kerf	Maximize	150	750	3
	Bottom kerf	Minimize	150	450	4
	HAZ	Minimize	262.5	712.5	4
	Alpha Angle	Minimize	0	5.35	2
Criteria 4	Top Kerf	Maximize	150	750	4
	Bottom kerf	Minimize	150	450	4
	HAZ	Minimize	262.5	712.5	4
	Alpha Angle	Minimize	0	5.35	3
Criteria 4	Top Kerf	Maximize	150	750	5
	Bottom kerf	Minimize	150	450	5
	HAZ	Minimize	262.5	712.5	5
	Alpha Angle	Minimize	0	5.35	5

Table 13- Optimum prediction results and experimental validation

Solution	Input parameters			Composite desirability		Output parameters				
	Speed (mm/s)	Power (W)	FPP (mm)			Top Kerf (µm)	Bottom kerf (µm)	Ratio	HAZ (µm)	Alpha Angle (°)
1	6.84	30	1	0.9097	Abaqus	375	225	1.6666	279	2.68
					Predicted	361.858	230.791	0.99	289.14	2.37
					Error%	3.5	2.5	43.7	3.6	11.6
2	20	33.03	-1.85	0.9192	Abaqus	300	150	2	324	2.68
					Predicted	304.781	185.61	1.7	342.348	2.57
					Error%	2	23.3	15	5.6	4.1
3	12.87	30	1	0.9167	Abaqus	225	150	1.5	285	1.34
					Predicted	198.363	177.073	1.12	273.421	0.97
					Error%	11.8	18	25.3	39.1	27.6
4	12.40	30	1	0.9108	Abaqus	175	175	1	268	0.68
					Predicted	196.461	180.938	1.08	274.662	0.91
					Error%	12.2	3.4	8	2.5	33.8
5	12.08	30	1	0.9065	Abaqus	175	175	1	265	0.72
					Predicted	196.728	183.648	1.07	275.508	0.80
					Error%	14.4	4.9	7	3.4	11.1

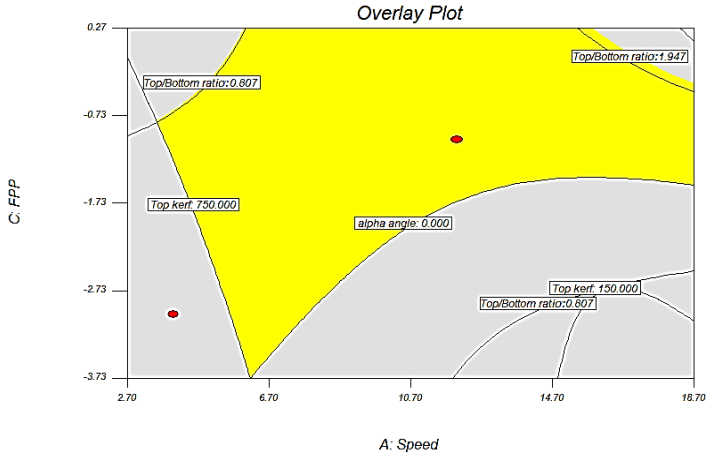

(a)

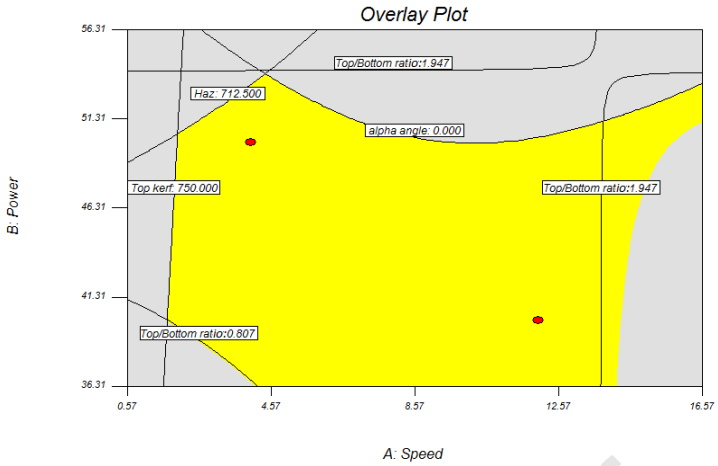

(b)

Figure 15 Overlay plot a) Laser FFP and cutting speed b) Laser power and cutting speed

5- Conclusion

In this study, a 3.2 mm thick polycarbonate sheet was selected. The laser used was a continuous mode low power CO_2 laser. The input parameters of the simulation included laser power, cutting speed, and laser focal plane position. Gas pressure (3 Bar) was also assumed for the polycarbonate material. The parameters of top kerf width, and the bottom kerf width, heat-affected zone, the ratio of the top kerf width to the bottom kerf width and alpha angle were considered as simulation output responses. The difference between the results of numerical simulation with experiments under similar conditions was less than 12%, which indicates appropriate modeling accuracy.

The results showed that the highest top kerf width occurs at the cutting speed of 4 mm/s and the focal plane distance of -3 from the workpiece, and the lowest kerf width is obtained when the focal plane position is at the deepest part of the workpiece at the position of 3 mm. It was shown that the laser cutting speed has a significant effect on the ratio of top kerf width to bottom kerf width, and by increasing the laser cutting speed from 4 to 20 mm/s, this ratio increases from 0 to 875.1 µm. Furthermore, by increasing the laser cutting speed from 4 to 20 mm/s, and decreasing the laser power from 50 to 20 W, the heat-affected zone decreases.

Declaration of interests

The authors declare that they have no known competing financial interests or personal relationships that could have appeared to influence the work reported in this paper.

References

[1] S. M. Karazi, M. Moradi, and K. Y. Benyounis, *Statistical and Numerical Approaches for Modeling and Optimizing Laser Micromachining Process-Review*. Elsevier Ltd., 2019.

[2] M. Moradi, O. Mehrabi, T. Azdast, and K. Y. Benyounis, "Enhancement of low power CO_2 laser cutting process for injection molded polycarbonate," *Opt. Laser Technol.*, vol. 96, pp. 208–218, 2017, DOI: 10.1016/j.optlastec.2017.05.022.

[3] B. El Aoud, M. Boujelbene, E. Bayraktar, S. Ben Salem, and I. Miskioglu, "Studying Effect of CO 2 Laser Cutting Parameters of Titanium Alloy on Heat-Affected Zone and Kerf Width Using the Taguchi Method," vol. 6, pp. 143–150, 2018, DOI: 10.1007/978-3-319-63408-1.

[4] M. Kurt, Y. Kaynak, and E. Bagci, "Dimensional analyses and surface quality of the laser cutting process for engineering plastics," pp. 259–267, 2009, DOI: 10.1007/s00170-008-1468-7.

[5] S. Marimuthu, J. Dunleavey, Y. Liu, M. Antar, and B. Smith, "Laser cutting of aluminium-alumina metal matrix composite," *Opt. Laser Technol.*, vol. 117, no. February, pp. 251–259, 2019, DOI: 10.1016/j.optlastec.2019.04.029.

[6] M. Sharifi and M. Akbari, "Experimental investigation of the effect of process parameters on cutting region temperature and cutting edge quality in laser cutting of AL6061T6 alloy," *Optik (Stuttg).*, vol. 184, pp. 457–463, 2019, DOI: 10.1016/j.ijleo.2019.04.105.

[7] M. S. Shaikh Mohammad Meiabadi, A. Kazerooni, M. Moradi, and M. J. Torkamany, "Laser-assisted joining of St12 to polycarbonate: Experimental study and numerical simulation," *Optik (Stuttg).*, p. 164151, 2019, DOI: 10.1016/j.ijleo.2019.164151.

[8] M. H. El-Hofy, and H. El-Hofy, "Laser beam machining of carbon fiber-reinforced composites: a review," *Int. J. Adv. Manuf. Technol.*, vol. 101, no. 9–12, pp. 2965–2975, 2019, DOI: 10.1007/s00170-018-2978-6.

[9] A. M. Varsi, and A. H. Shaikh, " Experimental and statistical study on kerf taper angle during CO 2 laser cutting of thermoplastic material ," *J. Laser Appl.*, vol. 31, no. 3, p. 032010, 2019, DOI: 10.2351/1.5087846.

[10] E. Haddadi, M. Moradi, A. Karimzad Ghavidel, A. Karimzad Ghavidel, and S. Meiabadi, "Experimental and parametric evaluation of cut quality characteristics in CO2 laser cutting of polystyrene," *Optik (Stuttg).*, vol. 184, no. February, pp. 103–114, 2019, DOI: 10.1016/j.ijleo.2019.03.040.

[11] X. Chen, T. Li, K. zhai, Z. Hu, and M. Zhou, "Using orthogonal experimental method optimizing the surface quality of CO2 laser cutting process for PMMA microchannels," *Int. J. Adv. Manuf. Technol.*, vol. 88, no. 9–12, pp. 2727–2733, 2017, DOI: 10.1007/s00170-016-8887-7.

[12] S. J. S. Al-Qaisy, and C. Karataş, "Laser cutting of high-density poly ethylene (Hdpe) pipes Pe100 using Co2 gas laser," *Int. J. Eng. Adv. Technol.*, vol. 9, no. 1, pp. 6193–6199, 2019, DOI: 10.35940/ijeat.A1783.109119.

[13] C. M. Gruescu, C. L. Ionescu, I. Nicoara, and A. Lovasz, "Experimental optimization of process parameters in laser cutting of polycarbonate gears," *Mechanika*, vol. 18, no. 2, pp. 233–238, 2012, DOI: 10.5755/j01.mech.18.2.1561.

[14] A. M. Varsi, and A. H. Shaikh, " Developing an algorithm for predicting depth as well as a number of passes during CO 2 laser machining on thermoplastic material ," *J. Laser Appl.*, vol. 30, no. 4, p. 042007, 2018, DOI: 10.2351/1.5048055.

[15] S. Sihn, J. Pitz, R. H. Gerzeski, A. K. Roy, and J. P. Vernon, "Experimentally-validated computational model for temperature evolution within laser heated fiber-reinforced polymer matrix composites," *Compos. Struct.*, vol. 207, pp. 966–973, 2019, DOI: 10.1016/j.compstruct.2018.09.041.

[16] T. Ohkubo, M. Tsukamoto, and Y. Sato, "Numerical simulation of laser beam cutting of carbon fiber reinforced plastics," *Phys. Procedia*, vol. 56, no. C, pp. 1165–1170, 2014, DOI: 10.1016/j.phpro.2014.08.031.

[17] B. S. Yilbas, S. S. Akhtar, C. Karatas, H. Ali, and N. Abu-Dheir, "Laser Cutting of Holes in Inconel 803 Alloy and Analysis of Thermal Stress Field," *Mach. Sci. Technol.*, vol. 23, no. 1, pp. 95–117, 2019, DOI: 10.1080/10910344.2018.1486412.

[18] E. H. Amara *et al.*, "Simulation by temperature gradient adaption of wavelength effect in metal laser cutting," *J. Laser Appl.*, vol. 29, no. 2, p. 022209, 2017, DOI: 10.2351/1.4983264.

[19] V. Pata, L. Sýkorová, O. Šuba, and M. KubiŠová, "Simulation of the Transient Temperature Field when Laser Machining Polymeric Materials," *Key Eng. Mater.*, vol. 686, no. 1, pp. 246–251, 2016, DOI: 10.4028/www.scientific.net/KEM.686.246.

[20] Y. Ayed, G. Germain, W. Ben Salem, and H. Hamdi, "Experimental and numerical study of laser-assisted machining of Ti6Al4V titanium alloy," *Finite Elem. Anal. Des.*, vol. 92, pp. 72–79, 2014, DOI: 10.1016/j.finel.2014.08.006.

[21] J. Meško, A. Zrak, R. Nigrovič, and M. Žmindák, "Finite element simulation of laser cutting process of steel sheet," *MATEC Web Conf.*, vol. 157, pp. 2–7, 2018, DOI: 10.1051/matecconf/201815702030.

[22] K. Kheloufi, E. H. Amara, and A. Benzaoui, "Numerical simulation of transient three-dimensional temperature and kerf formation in laser fusion cutting," *J. Heat Transfer*, vol. 137, no. 11, pp. 1–9, 2015, DOI: 10.1115/1.4030658.

[23] A. Ottoa and M. Schmidta, "Towards a universal numerical simulation model for laser material processing," *Phys. Procedia*, vol. 5, no. PART 1, pp. 35–46, 2010, DOI: 10.1016/j.phpro.2010.08.120.

[24] M. Benton, M. R. Hossan, P. R. Konari, and S. Gamagedara, "Effect of process parameters and material properties on laser micromachining of microchannels," *Micromachines*, vol. 10, no. 2, 2019, DOI: 10.3390/mi10020123.

[25] G. Le, A. Hoang, D. Nguyen, M. Nguyen, and Q. Nguyen, "A Method to Determine Machining Parameters for Laser Cutting Machine Using Numerical Simulation," vol. 2, no. 9, pp. 65–68, 2018.

[26] M. Moradi, and E. Golchin, "Investigation on the effects of process parameters on laser percussion drilling using finite element methodology; statistical modeling and optimization," *Lat. Am. J. Solids Struct.*, vol. 14, no. 3, pp. 464–484, 2017, DOI: 10.1590/1679-78253247.

[27] V. Tangwarodomnukun, and S. Mekloy, "Temperature field modeling and cut formation in laser micromachining of silicon in ice layer," *J. Mater. Process. Technol.*, vol. 271, no. October 2018, pp. 202–213, 2019, DOI: 10.1016/j.jmatprotec.2019.04.006.

[28] S. Choi, and K. Y. Jhang, "Numerical study on thermal stress cutting of silicon wafers using two-line laser beams," *J. Mech. Sci. Technol.*, vol. 33, no. 8, pp. 3621–3627, 2019, DOI: 10.1007/s12206-019-0702-6.

[29] Paul, B.K., Ahmed, K., Vigneswaran, D., Ahmed, F., Roy, S., and Abbott, D. Quasi-photonic crystal fiber-based spectroscopic chemical sensor in the terahertz spectrum: Design and analysis. *IEEE Sensors Journal*, 18(24), pp.9948-9954, 2018, DOI: 10.1109/JSEN.2018.2872892.

[30] Jabin, M.A., Ahmed, K., Rana, M.J., Paul, B.K., Islam, M., Vigneswaran, D., and Uddin, M.S. Surface plasmon resonance-based titanium coated biosensor for cancer cell detection. *IEEE Photonics Journal*, 11(4), pp.1-10, 2019, DOI: 10.1109/JPHOT.2019.2924825.

[31] Ahmed, K., Haque, M.J., Jabin, M.A., Paul, B.K., Amiri, I.S., and Yupapin, P., Tetra-core surface plasmon resonance based biosensor for alcohol sensing. *Physica B: Condensed Matter*, 570, pp.48-52, 2019, DOI: 10.1016/j.physb.2019.05.047.

[32] Ahmed, K., Paul, B.K., Jabin, M.A., and Biswas, B., FEM analysis of birefringence, dispersion, and nonlinearity of graphene-coated photonic crystal fiber. *Ceramics International*, 45(12), pp.15343-15347, 2019, DOI: 10.1016/j.ceramint.2019.05.027.

[33] Paul, B.K., Chakma, S., Khalek, M.A., and Ahmed, K., Silicon nanocrystal filled ellipse core-based quasi photonic crystal fiber with birefringence and very high nonlinearity. *Chinese Journal of Physics*, 56(6), pp.2782-2788, 2018, DOI: 10.1016/j.cjph.2018.09.030.

[34] Thenmozhi, H., Rajan, M.M., and Ahmed, K., D-shaped PCF sensor based on SPR for the detection of

carcinogenic agents in food and cosmetics. *optik*, 180, pp.264-270, 2019, DOI: 10.1016/j.ijleo.2018.11.098.

[35] Li, M., Gan, G., Zhang, Y. and Yang, X, "Thermal defect characterization and strain distribution of CFRP laminate with open hole following fiber laser cutting process," *Optics & Laser Technology*, 2020, p.105891, DOI: 10.1016/j.optlastec.2019.105891, 122.

[36] Kaselouris, E., Baroutsos, A., Papadoulis, T., Papadogiannis, N.A., Tatarakis, M. and Dimitriou, V., 2020. A Study on the Influence of Laser Parameters on Laser-Assisted Machining of Aisi H-13 Steel. In Key Engineering Materials, Vol. 827, pp. 92-97, DOI: 10.4028/www.scientific.net/KEM.827.92.

[37] R. Akarapu, B. Q. Li, and A. Segall, "A Thermal Stress and Failure Model for Laser Cutting and Forming Operations," vol. 4, no. October, pp. 51–62, 2004, DOI: 10.1361/15477020420756.

[38] M. J. Kim, "3D finite element analysis of evaporative laser cutting," vol. 29, pp. 938–954, 2005, DOI: 10.1016/j.apm.2005.02.015.

[39] M. Moradi, M. Karami Moghadam, M. Shamsborhan, M. Bodaghi, H. Falavandi, Post Processing of FDM 3D Printed Poly Lactic Acid Parts by Laser Beam Cutting, *polymers*, 2020.

[40] M. Moradi, and M. Karami moghadam, "High power diode laser surface hardening of AISI 4130 ; statistical modeling and optimization," *Opt. Laser Technol.*, vol. 111, no. October 2018, pp. 554–570, 2019, DOI: 10.1016/j.optlastec.2018.10.043.